Heliyon 10 (2024) e37985

Contents lists available at ScienceDirect

Heliyon

journal homepage: www.cell.com/heliyon

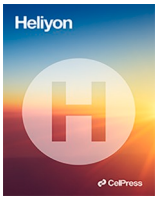

Research article

Identification of a novel prognostic model for gastric cancer utilizing glutamine-related genes

Weidong Li [a], Qixing Zhong [a], Naisheng Deng [a], Haitao Wang [a], Jun Ouyang [a], Zhifen Guan [a], Xinhao Zhou [a], Kai Li [a], Xueying Sun [b,**], Yao Wang [a,*]

[a] Department of Gastrointestinal Surgery, Zhongshan City People's Hospital, Zhongshan, 528400, Guangdong, China
[b] Department of Molecular Medicine & Pathology, Faculty of Medical and Health Sciences, the University of Auckland, Auckland, 1142, New Zealand

ARTICLE INFO

Keywords:
Gastric cancer
Glutamine metabolism
Bioinformatic
Risk model

ABSTRACT

Background: Glutamine metabolism presents a promising avenue for cancer prevention and treatment, but the underlying mechanisms in gastric cancer (GC) progression remain elusive.
Methods: The TCGA-STAD and GEO GSE62254 datasets, containing gene expression, clinical information, and survival outcomes of GC, were meticulously examined. Differential expression analysis and weighted gene co-expression network analysis (WGCNA) were employed to excavate a key module (MEturquoise), which was used to intersect with glutamine metabolism-related genes (GMRGs) and differentially expressed genes (DEGs) to identify differentially expressed GMRGs (DE-GMRGs). LASSO and Cox Univariate analyses were implemented to determine risk model genes. Correlation of the risk model with clinical parameters, pathways, and tumor immune microenvironments, was analyzed, and its prognostic independence was validated by Cox analyses. Finally, reverse transcription-quantitative polymerase chain reaction (RT-qPCR) was performed to validate the expression levels of MYB, LRFN4, LMNB2, and SLC1A5 in GC and para-carcinoma tissue.
Results: The excavation of 4521 DEGs led to the discovery of the key MEturquoise module, which exhibited robust correlations with GC traits. The intersection analysis identified 42 DE-GMRGs, among which six genes showed consistency. Further LASSO analysis established *MYB*, *LRFN4*, *LMNB2*, and *SLC1A5* as pivotal risk model genes. The risk model demonstrated associations with oncogenic and metabolism-related pathways, inversely correlating with responses to immune checkpoint blockade therapies. This risk model, together with "age", was validated to be an independent prognostic factor for GC. RT-qPCR result indicated that *MYB*, *LRFN4*, *LMNB2*, and *SLC1A5* expressions were remarkably up-regulated in GC tissues comparison with para-carcinoma tissue.
Conclusion: The present study has generated a novel risk module containing four DE-GMRGs for predicting the prognosis and the response to immune checkpoint blockade treatments for GC. This risk model provides new insights into the involvement of glutamine metabolism in GC, warranting further investigation.

* Corresponding author.
** Corresponding author.
E-mail addresses: k.sun@auckland.ac.nz (X. Sun), tongjimc@126.com (Y. Wang).

https://doi.org/10.1016/j.heliyon.2024.e37985
Received 16 March 2024; Received in revised form 23 August 2024; Accepted 16 September 2024
Available online 19 September 2024

1. Introduction

Gastric cancer (GC) is the 5th most common cancer and the 4th leading cause of cancer-related death, remaining a major global health problem [1,2]. Globally, regions such as Asia, Eastern Europe, and Central and South America have a high incidence of GC [3]. Although early detection and targeted interventions have facilitated a reduction in GC mortality, the overall survival (OS) rate has not increased significantly, particularly for patients with advanced GC. The 5-year survival rate of late-stage patients is only about 10 % [4]. Therefore, understanding the mechanisms of disease progression and seeking novel effective prognostic factors and molecular targets are of great significance for improving the long-term survival for GC patients.

Recent studies reveal that amino acids intermediate metabolites that fuel biological metabolic pathways for sustaining tumor growth and progression [5]. Glutamine, the most abundant non-essential amino acid in human blood, can be hydrolyzed into glutamic acid by glutaminase, converted into α-ketoglutarate through deamidation, and then used as glutamine-derived carbon entry into the tricarboxylic acid cycle [6]. In addition to glucose, proliferating cancer cells also rely on glutamine as a major source of energy, which is known as glutamine addiction [7]. Tumor cells consume glutamine at a rate 5 to 10 times higher than normal cells. Glutamine metabolism supports fatty acid synthesis through reductive carboxylation, promoting lipid synthesis and regulating the expression levels of reactive oxygen species, which are beneficial to cancer cell growth [8]. Glutamine also plays an important role in the synthesis of the endogenous antioxidant glutathione, which can effectively inhibit the stress response of autoimmunity, thus protecting cells from oxidative damage [9]. Due to its critical biosynthetic and energy-generating roles in cancer progression, glutamine metabolism has become a promising target for cancer prevention and therapy [10,11]. Highly active glutamine decomposition supporting energy has been found in gastric cancer tissues [12], and inhibition of glutamine metabolism can suppress tumor growth [13] or enhance therapeutic efficacy in GC [14]. These studies have further emphasized the importance of glutamine metabolism in the progression of GC.

Immunotherapies, particularly immune checkpoint blockade treatments, have become the most promising strategies for cancers [15]. However, the clinical benefits of such immunotherapy in GC patients are limited, with notable side effects and high costs [15]. Metabolically hostile tumor microenvironments impose barriers to immune effector cells, impeding clinical remission through immunotherapy [16]. Metabolic communication between cancer cells and the neighboring immune cells determines the amplitude of antitumor immune responses. Glutamine antagonists have been developed and investigated for cancer treatments, particularly as a "metabolic checkpoint" for tumor immunotherapy [9]. However, the mechanisms underlying how glutamine metabolism influences the efficacy of cancer immunotherapy remains unclear.

It is known that hundreds of genes participate in regulating glutamine metabolism. Therefore, it is worthwhile digging out the key genes for unveiling the novel molecular targets for GC. Further mechanistic exploration of glutamine metabolism-related genes may help identify novel molecules for predicting the prognosis of GC patients. In the present study, we have employed multiple bioinformatics tools to analyze the glutamine metabolism-related genes (GMRGs) extracted from public databases, and finally excavated a novel glutamine metabolism related risk module (containing four GMRGs, i.e., *MYB*, *LRFN4*, *LMNB2*, and *SLC1A5*) for GC. Further analyses revealed that this risk model might be independent prognostic factor, correlated with the metabolism related pathways, and participated in the regulation of tumor immune microenvironments.

2. Materials and methods

2.1. Data sources

The RNA sequencing data for the TCGA-STAD dataset, which includes 350 tumor samples and 32 normal samples, as well as the clinical information of gastric cancer patients, were sourced from The Cancer Genome Atlas (TCGA) database (https://cancergenome.nih.gov/abouttcga/overview). The chip data of the GSE62254 dataset, containing the survival information of 300 tumor samples, was obtained from the Gene Expression Omnibus (GEO) database (https://www.ncbi.nlm.nih.gov/gds). Using "Glutamine Metabolism" as the key word, we extracted 118 and 1318 GMRGs (score >5, https://genecards.weizmann.ac.il/v3/) from the molecular signatures database (https://www.gsea-msigdb.org/gsea/msigdb/index.jsp) and Genecards database, respectively. After de-duplication, a total of 1351 GMRGs were obtained [17].

2.2. Differential expression analysis and weighted gene co-expression network analysis (WGCNA)

The R package DESeq2 (version 1.34.0) was used to identify differentially expressed genes (DEGs) between tumor and normal samples from the TCGA-STAD dataset [18] with criteria set at $|\log_2 FC| > 1$ and adj. $P < 0.05$. These sample groups were considered as traits for WGCNA. Initially, outliers were eliminated by clustering the samples to enhance analysis accuracy. A soft threshold was established to ensure gene interactions adhered to the scale-free distribution. The dissimilarity coefficient was introduced by calculating gene adjacency and similarity, which helped in obtaining the systematic clustering tree among genes. Modules were then screened based on the dynamic tree cutting criteria. Next, Pearson correlations of gene modules with traits were analyzed, and the module with the highest correlation with traits was identified as the key module. The module with the highest |cor| and significant p-value ($|cor|>0.5$, $p < 0.05$) was selected as the key module based on the correlation coefficient (cor). Finally, the relation between gene significance (GS) and module membership (MM) within the key module was calculated. The GMRGs, DEGs and key module genes were intersected to yield differentially expressed GMRGs (DE-GMRGs), which were further analyzed for Kyoto Encyclopedia of Genes and Genomes (KEGG) ($P < 0.05$) and gene ontology (GO) (adj. $P < 0.05$) enrichments by R package clusterProfiler (version 4.0.5) [19].

2.3. Construction of the risk model

In the TCGA-STAD dataset, Cox univariate regression analysis was conducted on DE-GMRGs for identifying genes with HR≠1 and $P < 0.05$. These genes were then analyzed using the least absolute shrinkage and selection operator (LASSO) method to identify risk model genes, forming the basis for constructing a risk model. The risk score for each GC sample in the TCGA-STAD dataset was calculated. GC samples were categorized into low- and high -risk groups according to median risk score. Survival differences were evaluated by survival analysis. The receiver operating characteristic (ROC) curve was plotted to assess the prognostic risk model's prediction accuracy. The results were further validated using the same assays in the GSE62254 dataset. Finally, the mutation status of the TCGA-STAD dataset and risk model genes in GC samples was analyzed using the R package maftools (version 2.10.5) [20].

2.4. Correlation analysis of the risk score and clinical indicators

The relationship of the risk score with each clinical parameter (age, gender, stages, TNM [T: tumor; N: lymph node; M: metastasis] staging system, grade) in TCGA-STAD dataset was analyzed. Subsequently, KEGG and GO functional enrichment analyses were conducted on groups with varying risk levels using R package GSVA (Gene Set Variation Analysis) (version 1.42.0) [21].

2.5. Correlation analysis of risk score and oncogenic pathways

Thirteen oncogenic pathways were identified based on the relevant genetic signature data provided by Sanchez-Vega and Mariathasan (Supplementary Table S1), and their differences between these groups with varying risk levels were analyzed by the ssGSEA in TCGA-STAD dataset. Finally, the correlations between risk score and oncogenic pathways were analyzed by Spearman correlation analysis.

2.6. Correlation analysis of risk score and factors involved in tumor immune microenvironments

The relationship between the factors composing tumor immune microenvironments and risk score was analyzed in TCGA-STAD dataset. First, three metabolism-related scores (immune, stromal, and ESTIMATE scores) were compared between groups with varying risk levels, followed by the comparisons of the proportion of immune cells, the immune response gene set, and the 48 immune checkpoints, by Wilcoxon rank-sum test. Then, Spearman correlation analysis was implemented between significantly different immune cells, risk model genes, risk score, immune response gene sets and immune checkpoints, respectively. The tumor immune dysfunction and exclusion (TIDE) scores of the low - and high -risk groups were evaluated for assessing the prognostic effect of immune checkpoint inhibition therapy. Next, the immunophenotype scores (IPS) were gained via The Cancer lmaging Archive (TCIA) database (TCIA https://tcia.at), and their differences between the low- and high-risk groups were compared. Finally, the Spearman correlation between PD-1 expression for each GC tissue and the risk score was analyzed in the TCGA-STAD dataset, in which the GC tissues were categorized into the low and high PD-1 expression groups, the survival analysis of these two groups was carried out. The relationship and predictive power of the risk score with anti-PD-L1 therapy efficacy were analyzed by utilizing the immunotherapy dataset (IMvigor210).

2.7. Independent prognostic analysis

In the TCGA-STAD dataset, the risk score and clinical parameters were analyzed using univariate Cox analysis with the R package survival (version 3.2–13) [22], factors with $P < 0.05$ were then subjected to multivariate Cox analysis to identify independent prognostic factors. A nomogram was constructed to predict patient survival probabilities at 1, 2, and 3 years, and calibration curves were drawn to validate the results. Finally, the expression levels of risk model genes were compared between normal and tumor samples in the TCGA-STAD dataset.

2.8. Collection and processing of samples

A total of six gastric cancer (GC) tissue samples, together with corresponding para-carcinoma tissue specimens, was obtained from People's Hospital of Zhongshan. This research was implemented in rigorous adherence to the ethical guidelines delineated in the World Medical Association Declaration of Helsinki. Prior ethical approval had been secured from the Ethics Committee of Zhongshan City People's Hospital (2023-070); all participating patients provided informed consent. None of the tissue specimens had undergone preoperative radiotherapy or chemotherapy exposure. Immediately upon surgical excision, the samples were preserved at −80 °C with RNA stabilization solution for subsequent analysis.

2.9. RT-qPCR assay

Total RNA was carefully isolated from six matched GC tissues and para-carcinoma tissues, which were snap-frozen with liquid nitrogen, using TRIzol reagent (Biomed, China). Then, RNA was diluted according to its concentration and reverse-transcribed into complementary DNA (cDNA) by commercial reverse transcription kit (Biomed, China). Quantitative real-time PCR (qRT-PCR) was applied on the AutoMolec 1600 (Antobio, China). The thermocycling conditions were set as follows: 180 s at 95 °C, followed by 40

cycles of denaturation for 15 s at 95 °C, then, 60 s at 60 °C. Primer sequences used in this study are detailed in Supplementary Table S2. Relative mRNA expression levels were determined using the $2^{-\Delta\Delta Ct}$ method, with GAPDH as the housekeeping gene for normalization. The Mann-Whitney *U* test and Student's t-test were used to compare two groups, with $p < 0.05$ considered significant. Pearson's correlation coefficient ® assessed the relation between the gene expression and risk score. Gene expression data were log2-transformed after adding one to each value.

3. Results

3.1. DEGs and the key module identification

4521 DEGs were identified from tumor and normal samples (Fig. 1A, Supplementary Table S3), and the top 10 down- and up-regulated genes are illustrated in the heat map (Fig. 1B). The statistical population exhibited good overall clustering (Fig. 1C), so no samples needed to be excluded. Based on the red line in Fig. 1D, the soft threshold was set at 8. At this threshold, the vertical coordinate R^2 exceeded 0.85, and the mean adjacency function value approached 0, indicating the network was nearly scale-free and showed a flat trend. Subsequently, 12 modules were identified by constructing the co-expression matrix in Fig. 1E. Finally, the MEturquoise module containing 4016 genes was selected as the key module because it had the most significant correlation with traits ($|Cor| > 0.5$ and $P < 0.05$) (Fig. 1F). This module also showed a very strong correlation with gene significance for tumors (Fig. 1G).

3.2. Functional pathways involved in DE-GMRGs

The overlapping analysis of GMRGs, DEGs and genes in the key module genes yielded 42 DE-GMRGs (Fig. 2A). These DE-GMRGs were involved in various GO entries. Sorted by the number of target genes as a proportion of all genes and the size of the P-value, the GO entries included 'chromosomal region', 'folic acid-containing compound metabolic process', 'nucleobase metabolic process', 'nucleoside monophosphate biosynthetic process', and 'oxygen carrier activity'(Fig. 2B). DE-GMRGs were also enriched in KEGG pathways. Sorted by the number of target genes as a proportion of all genes and the size of the P-value, the KEGG pathways included 'alanine, aspartate and glutamate metabolism', 'pyrimidine metabolism', 'cysteine and methionine metabolism', 'glycine, serine and threonine metabolism', and 'DNA replication' (Fig. 2C).

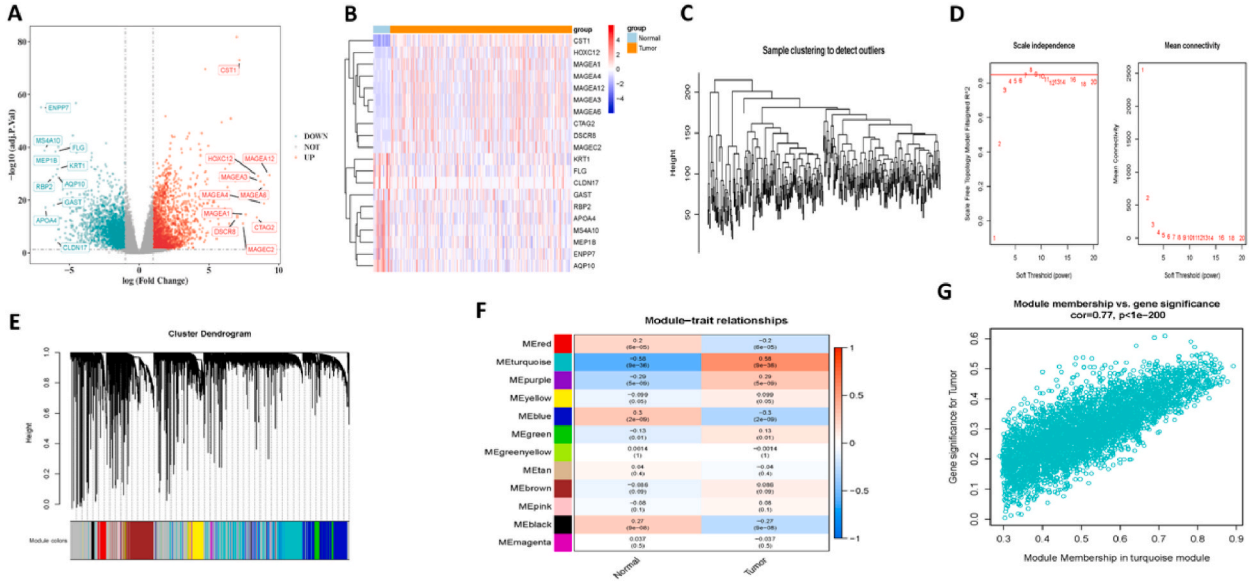

Fig. 1. Identification of DEGs and Key Module. (A) The volcano plot displays DEGs between tumor and normal samples. (B) The heat map highlights the top 10 up-regulated and down-regulated genes, with red represents for high expression and blue represents for low expression in tumor samples compared to normal samples. (C) The sample clustering tree confirms that all samples were included in the network construction. (D) Network topology analysis for various soft-thresholding powers is shown. The left panel illustrates the scale-free fit index (y-axis) as a function of the soft-thresholding power (x-axis), while the right panel shows the mean connectivity (degree, y-axis) as a function of the soft-thresholding power (x-axis). (E) Cluster dendrograms depict gene groups identified using weighted gene co-expression network analysis within TCGA-STAD datasets, with assigned module colors. (F) Module-trait relationships of significant modules, showing correlation values to normal and tumor subtype phenotypes, were calculated. Each row represents a module eigengene, and each column represents a trait. Each cell contains the corresponding correlation and P-value, with the correlation indicated by color. (G) A scatterplot of gene significance versus module membership in the turquoise module is shown. (For interpretation of the references to color in this figure legend, the reader is referred to the Web version of this article.)

Fig. 2. Screening and analysis of functional pathways involved in DE-GMRGs. (A) Overlapping analysis of GMRGs, DEGs, and key module genes. (B) GO analysis of functional pathways involved in the DE-GMRGs. The overall distinction is made into 3 parts: BP, CC, and MF. The horizontal axis is the number of genes enriched in GO entries as a proportion of all genes, and the vertical axis is the name of the corresponding entry. The red and blue gradient indicates the p-value change. (C) KEGG analysis for DE-GMRGs. The Sankey diagram is on the left while bubble diagram is on the right. (For interpretation of the references to color in this figure legend, the reader is referred to the Web version of this article.)

3.3. Risk models construction

3.3.1. Risk model evaluation

The Cox univariate analysis demonstrated that six genes (*DNMT1*, *LMNB2*, *FEN1*, *SLC1A5*, *LRFN4* and *MYB*) were consistent with HR≠1 and $P < 0.05$ (Fig. 3A). These genes were subjected to LASSO regression analysis and four of them (*MYB*, *LRFN4*, *LMNB2* and *SLC1A5*) were identified to be risk model genes (Fig. 3B). Survival samples were primarily clustered in regions with higher overall survival (OS) times and lower risk scores, while death samples had higher risk scores and lower OS times (Fig. 3C). Additionally, the Kaplan-Meier curves demonstrated that survival rates in the low-risk group were remarkably higher than high-risk group (Fig. 3D). The area under the curve (AUC) values for 1-year (AUC = 0.63), 2-year (AUC = 0.62), and 3-year (AUC = 0.62) were all above 0.6, suggesting the risk model's capability to evaluate the prognosis of GC patient (Fig. 3E). The above results generated in the TCGA-STAD dataset were consistent with those in the GSE62254 dataset (Supplementary Figure S). Fig. 3F illustrates the mutations in the samples of TCGA-STAD dataset. Moreover, the four risk model genes had different degrees of mutations, mainly involved deletion mutation and reading frame deletions (Fig. 3G).

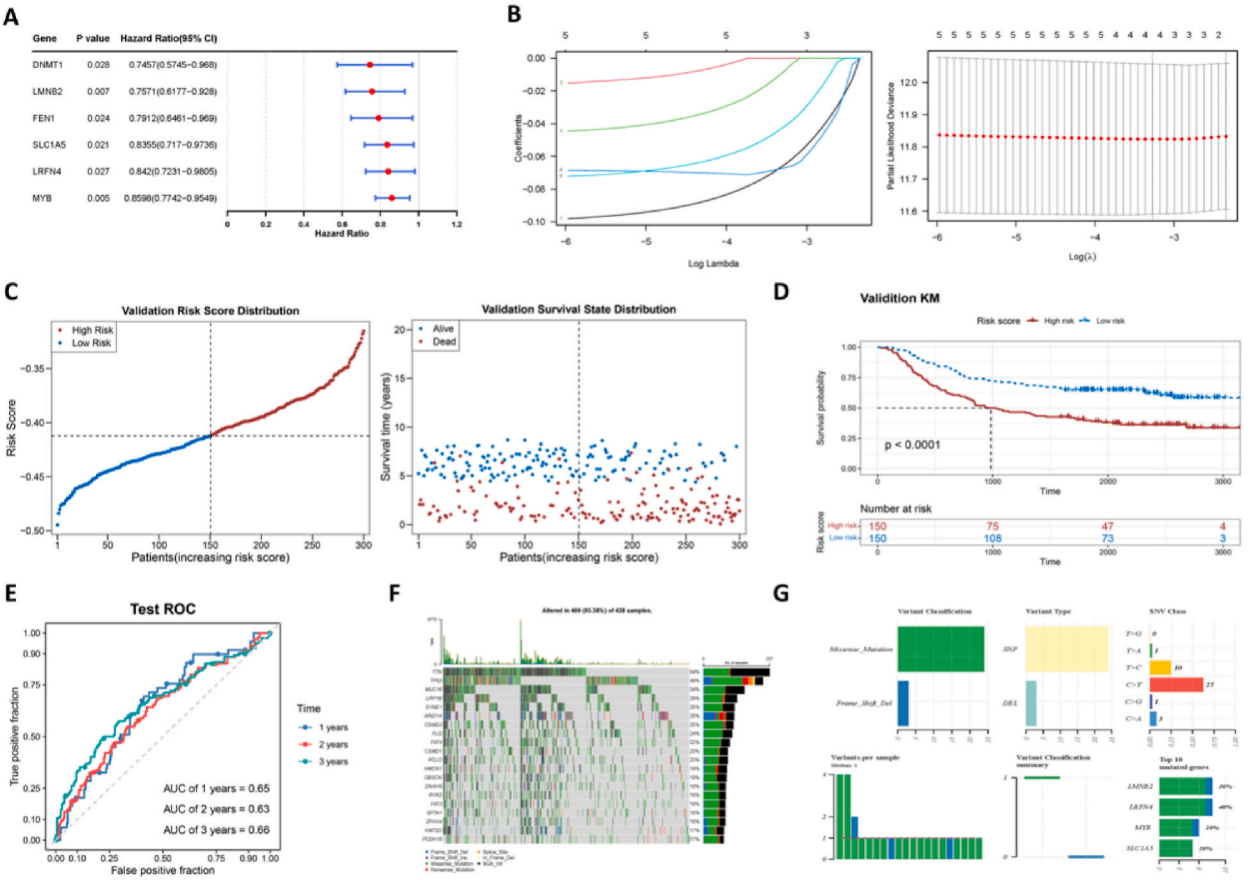

Fig. 3. Risk prognostic model construction for GC based on DE-GMRGs in the TCGA-STAD dataset. (A) One-factor Cox Forest plot of 6 genes associated with prognosis. (B) The partial likelihood deviance versus log (λ) was plotted by Cox LASSO regression model (left panel), and lambda parameter is used to describe the coefficients of selected features (right panel). 1 Black: MYB; 2 Red: FEN1; 3 Green: LRFN4; 4 Blue: LMNB2; 6 Sky Blue: SLC1A5. (C) Risk score analysis of four risk model genes. Patients were evenly divided into two groups based on the median risk score in the left panel, where the blue curve indicates the low-risk group, while the red one indicates the high-risk group. The survival status of patients is shown in the right panel, where red dots represent for death, while blue dots represent for survival. (D) The overall survival of the high-risk and low-risk groups is indicated by Kaplan-Meier (KM) survival curves. (E) The predictive efficiency of risk score is further verified via time-dependent ROC curves. (F) The top 20 mutated genes in the samples of TCGA-STAD dataset. One column corresponds to a sample, one row corresponds to a gene, and different colors distinguish different mutation types. (G) Mutation status of the risk model genes. From left to right, top to bottom in order: the above three graphs show the mutation type statistics. 1. Mutation classification 2. Mutation type. 3. Base substitutions. 4. The number of mutations per sample is counted; 5. Comprehensive statistics of mutation classification of samples 6. The vertical coordinate is the name of the gene, and the horizontal coordinate is the proportion of mutations in the gene. (For interpretation of the references to color in this figure legend, the reader is referred to the Web version of this article.)

3.3.2. The risk model was correlated with metabolism related pathways

The correlation analysis suggested that the risk scores differed remarkably in the subgroups of age and grade, indicating that the risk model correlated with patients' age and tumor grades (Fig. 4A). Additionally, high-risk group genes were primarily related to 'complement activation lectin pathway (GO)', 'positive regulation of smooth muscle cell differentiation (GO)', 'elastic fiber assembly (GO)', 'ECM receptor interaction (KEGG)', 'dilated cardiomyopathy (KEGG)', and 'calcium signaling pathway (KEGG)' (Fig. 4B). Meanwhile, low-risk group genes were primarily enriched to functional pathways including 'protein localization to nuclear body (GO)', 'positive regulation of chromosome segregation (GO)', 'mitotic DNA replication (GO)', 'glyoxylate and dicarboxylate metabolism (KEGG)', 'nucleotide excision repair (KEGG)', 'cell cycle (KEGG)' (Fig. 4C). Eventually, 12 cancer-related pathways were significantly different between these two groups (Fig. 4D), and risk score was shown to be strongly correlated with the oncogenic pathways (Fig. 4E).

3.3.3. The risk model was related to the tumor immune microenvironments

Subsequently, we explored in depth and compared tumor immune microenvironmental factors in groups with varying risk levels. The stromal score, immune score, and ESTIMATE score were significantly different between the high- and low-risk groups in Fig. 5A. In addition, the proportions of 28 immune cell subsets (Fig. 5B), 17 immune response gene sets (Fig. 5C), and 19 immune checkpoints

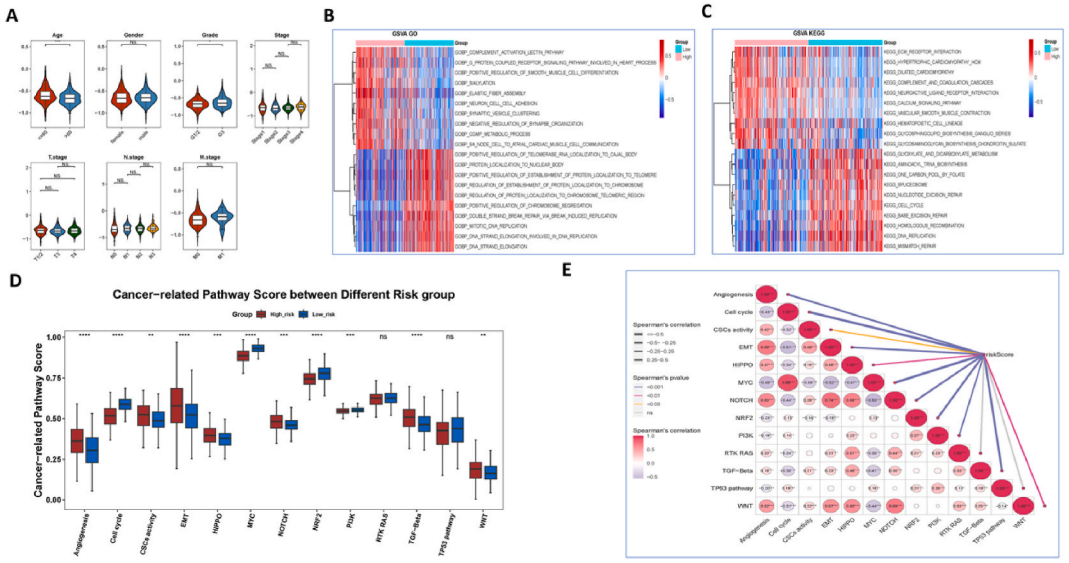

Fig. 4. Correlation analysis between the risk model and metabolism-related pathways. (A) Distribution of risk scores for clinical features of GC. The GO (B) KEGG (C) and functional enrichment analyses were conducted using GSVA. Red represents positive correlation while blue represents negative correlation. (D) The differences in 13 cancer-related pathways were analyzed by ssGSEA between the low-risk and high-risk groups. (E) The correlations between risk scores and 13 oncogenic pathways were analyzed using a Spearman correlation analysis, where red indicates positive correlation, while purple indicates negative correlation. "ns": no significance; "**": $P < 0.01$; "***": $P < 0.001$; "****": $P < 0.0001$. (For interpretation of the references to color in this figure legend, the reader is referred to the Web version of this article.)

(Fig. 5D) all significantly differed between the low- and high-risk groups.

We next further analyzed the correlation coefficients of model genes with related immune cells and genes. As shown in Fig. 6A, the four risk model genes demonstrated negative correlations with most of the significantly different immune cells, but showed positive correlations with activated memory B cells, $CD4^+$ T cells, and type 17 T helper cells. In particular, *MYB* was positively correlated with memory B cells, while *LRFN4* has inverse correlation with effector memory $CD4^+$ T cells. However, the risk score has positive correlation with most of the significantly different immune cells and showed the strongest positive association with mast cells, but

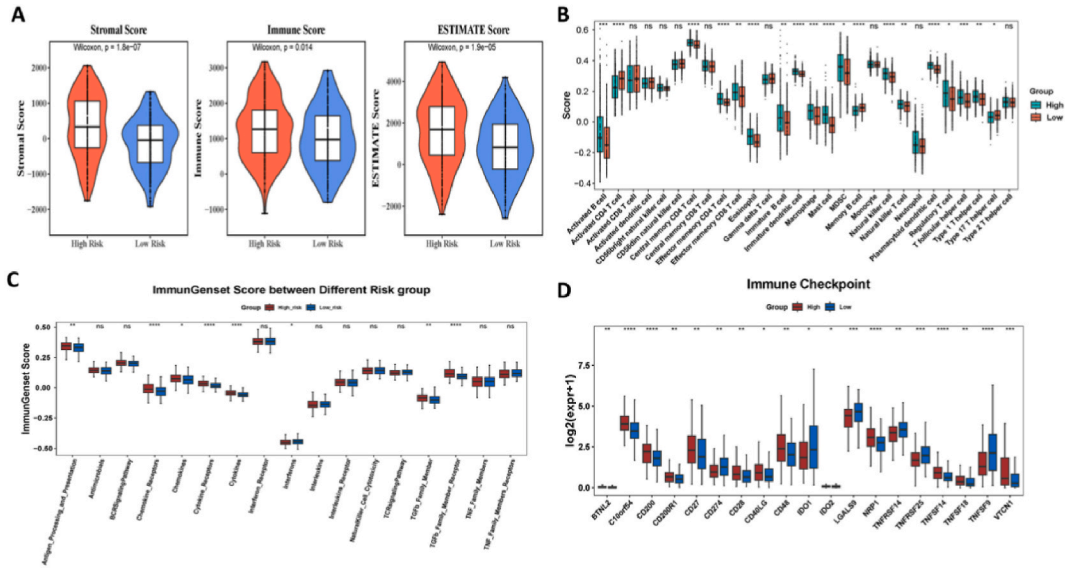

Fig. 5. Comparisons of factors involved in the tumor immune microenvironment in the high-risk and low-risk groups. Between the low and high risk groups, the immunization score, stromal score, and ESTIMATE score have been assessed for STAD patients. (A) Using the ssGSEA method, the proportion of 28 immune cells was calculated for samples from groups with varying risk levels. (B) According to ssGSEA, scores were calculated for each immune response gene set in different samples. (C) and 19 immune checkpoints (D) were compared between the groups with varying risk levels using Wilcoxon rank-sum test. "ns", no significance; "**", $P < 0.01$; "***", $P < 0.001$; "****", $P < 0.0001$.

negatively correlated with activated memory B cells and $CD4^+$ T cells (Fig. 6B). In addition, *MYB* had the strongest positive correlation with interferons, while *LRFN4* had the most significantly negative correlation with TGFb family member receptor (Fig. 6C). The lollipop chart suggested that the risk score has positive correlation with the majority of significantly different immune gene sets, and it had the most significant positive correlation with cytokines (Fig. 6D). The risk model genes were also negatively correlated with several significantly different immune checkpoints, such as *C10orf54* and *NRP1* (Fig. 6E).

Finally, we analyzed tumor immune dysfunction and rejection (TIDE), immunophenoscore (IPS) and PD-L1 immunotherapy prediction based on the risk model. As shown in Fig. 7A, TIDE score was significantly lower in the low-risk patients, suggesting that the high-risk patients were more resistant to the immune checkpoint blockade therapy. These results were not supported by the analysis of IPS, which showed no significant difference between these two groups (Fig. 7B). However, PD-1 expression had a significant negative correlation with risk scores (Fig. 7C). The survival of these two groups with either high or low PD-1 expression differed significantly, and the high-risk subgroup with low PD-1 expression had the shortest survival time (Fig. 7D). Furthermore, the risk scores were significantly and negatively correlated with the treatment response to anti-PD-L1 therapy. Specifically, the CR (complete response)/PR (partial response) group had significantly lower risk scores than the SD (stable disease)/PD (progressive disease) group (Fig. 7E).

3.4. Evaluation of risk model as the independent prognostic factor

Using a Cox univariate regression analysis, we showed the risk score, age, stage, and TNM staging system were significantly related to the survival with HR≠1 and $P < 0.05$ (Fig. 8A). Among these factors, the "age" and risk score were detected as independent

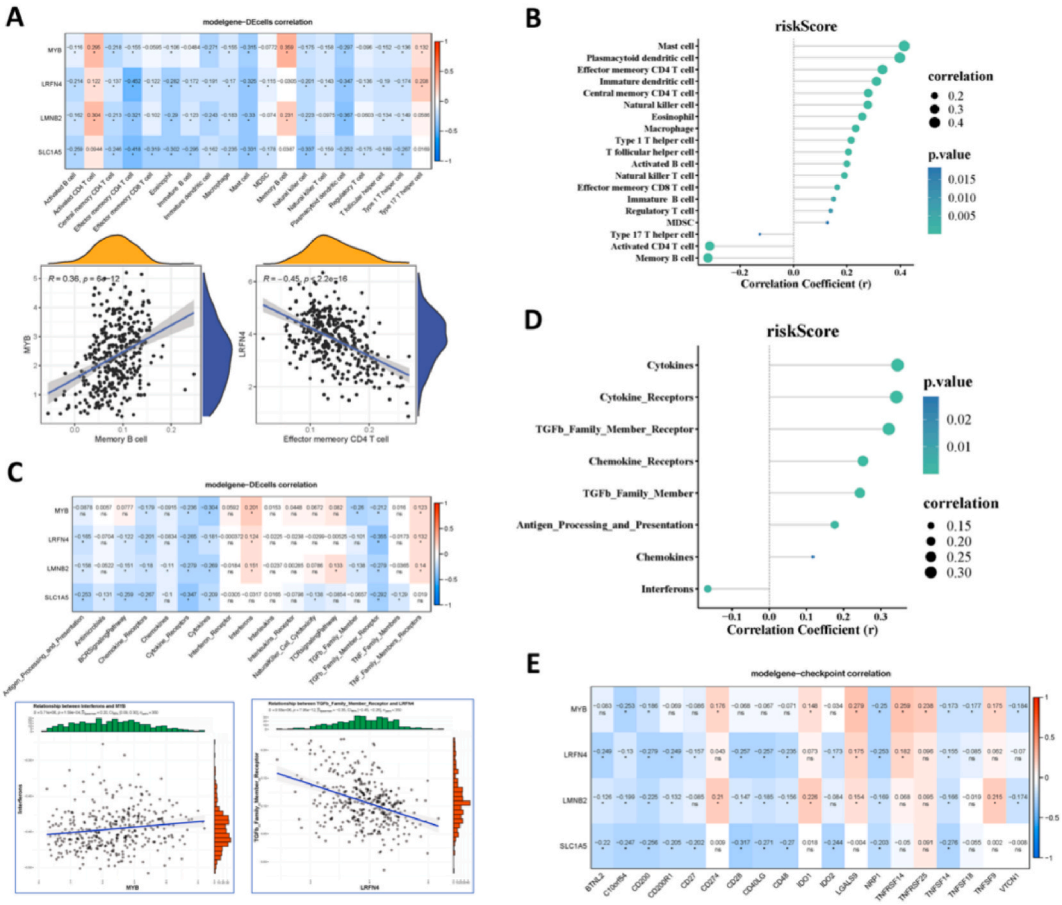

Fig. 6. Correlation analyses of the model genes with immune cells and genes. (A) The correlations between the differential immune cells and model genes are shown by a heat map (Upper panel). The correlations between *MYB* and memory B cells (left in the lower panel) and between *LRFN4* and effector memory CD4 T cells (right in the lower panels) are shown by scatter plots. (B) The correlations between risk scores and differential immune cells were analyzed by Spearman correlation analysis. (C) The correlations between the model genes and immune response gene sets are shown by a heat map (Upper panel). The correlations between *MYB*/interferon genes (left in the lower panel) and between *LRFN4* and TGFb family member receptor genes (right in the lower panels) are shown by scatter plots. (D) The correlations between risk scores and differential immune gene sets were analyzed using a Spearman correlation analysis. (E) The correlations between the model genes and differential immune checkpoints are shown by a heat map. In the heat maps, red represents a positive correlation, while blue represents a negative correlation. (For interpretation of the references to color in this figure legend, the reader is referred to the Web version of this article.)

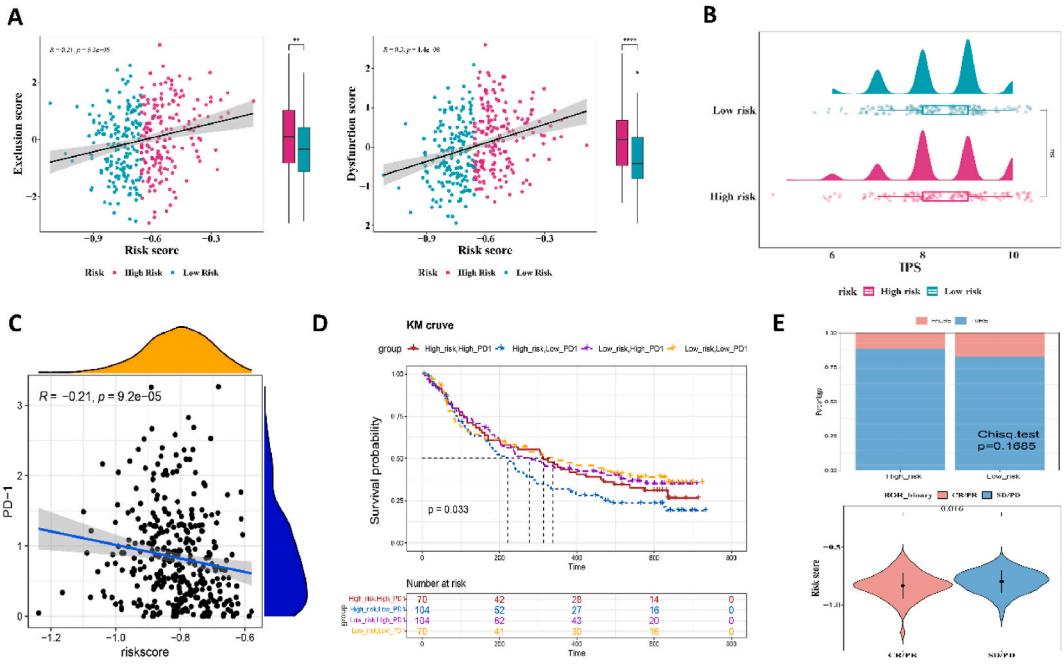

Fig. 7. Analyses of tumor immune dysfunction and exclusion (TIDE), immunophenotype score (Immunophenoscore, IPS) and PD-L1 immunotherapy prediction. (A) TIDE analysis shows that the exclusion and dysfunction scores were remakbaly lower in the low-risk patients by Wilcoxon rank-sum test. (B) IPS analysis shows there was no obvious changes in IPS scores between the groups with varying risk levels via Wilcoxon rank-sum test. (C) The correlation by a Spearman correlation analysis shows a significant negative correlation between PD-1 expression and risk score. (D) The survival of the above low-risk and high-risk groups with either a high or low expression of PD-1 is analyzed by the KM survival analysis, and the comparison was conducted via Log-Rank test. (E) Correlation analysis of risk scores and treatment response to anti-PD-L1 therapy. The upper panel shows the distribution of treatment response to anti-PD-L1 therapy in the high- and low-risk groups, while the lower panel shows the distribution of risk scores between the CR/PR and SD/PD groups. Comparison was performed by Wilcoxon rank-sum test. In above tests, $P < 0.05$ indicates a significant difference.

prognostic factors ($P < 0.05$) in the Cox multivariate regression analysis (Fig. 8A). The 1-/2-/3-year survival prognostic nomogram suggested that the risk score and "age" might has the potential to predict the prognosis of GC, and the calibration curve showed that the nomogram prediction probability perfectly matched the actual survival probability (Fig. 8B).These four risk model genes expressions were remarkably higher in tumor samples than in normal samples (Fig. 8C).

3.5. *Validation of the expression of four DE-GMRGs*

We examined the expression levels of four risk model genes (*MYB*, *LRFN4*, *LMNB2*, and *SLC1A5*) in gastric cancer (GC) and paracancerous tissue (PC). The results showed that *MYB*, *LRFN4*, *LMNB2*, and *SLC1A5* were significantly overexpressed in the GC group compared to the PC group (Fig. 9).

4. Discussion

The clinically used biomarkers like CEA and CA 19-9 in the diagnosis of GC lack the effectiveness in early detection [23]. The efficiency of newly discovered biomarkers like DNA methylation, PD-1 and PD-L1, and circulating tumor cells remains to be validated in clinical GC samples. Therefore, successfully finding potential prognostic biomarkers is critical for improving the prognosis of GC patient. The phenomenon of "glutamine dependence" in tumor cells implies an elevated demand for glutamine to support their rapid growth and proliferation [24]. At present, there is no direct evidence proving the influence of glutamine metabolism on the development and progression of GC, but the research in other digestive system tumors including HCC, pancreatic cancer and colorectal cancer, underscores the role of glutamine metabolism [25]. Metabolomics has found that the contents of glutamine and its derivatives, glutamic acid, were increased in GC tissues, indicating that glutamine metabolism may be involved in the progression of GC [26]. The tumorigenesis and progress of GC is accompanied by differential changes of small molecule metabolites such as glutamine [27], thus analyzing these differential changes may improve our understanding of disease progression and help in finding novel biomarkers for the early diagnosis and in seeking novel molecular targets for developing new treatments in the management of GC.

The present study has identified four risk model genes related to glutamine metabolism (*MYB*, *LRFN4*, *LMNB2*, and *SLC1A5*) through multiple bioinformatic analyses. The results may enhance our understanding of glutamine metabolism in GC. *MYB* gene encodes a ubiquitous direct transcription factor, which regulates the proliferation, growth, differentiation and survival of various cell

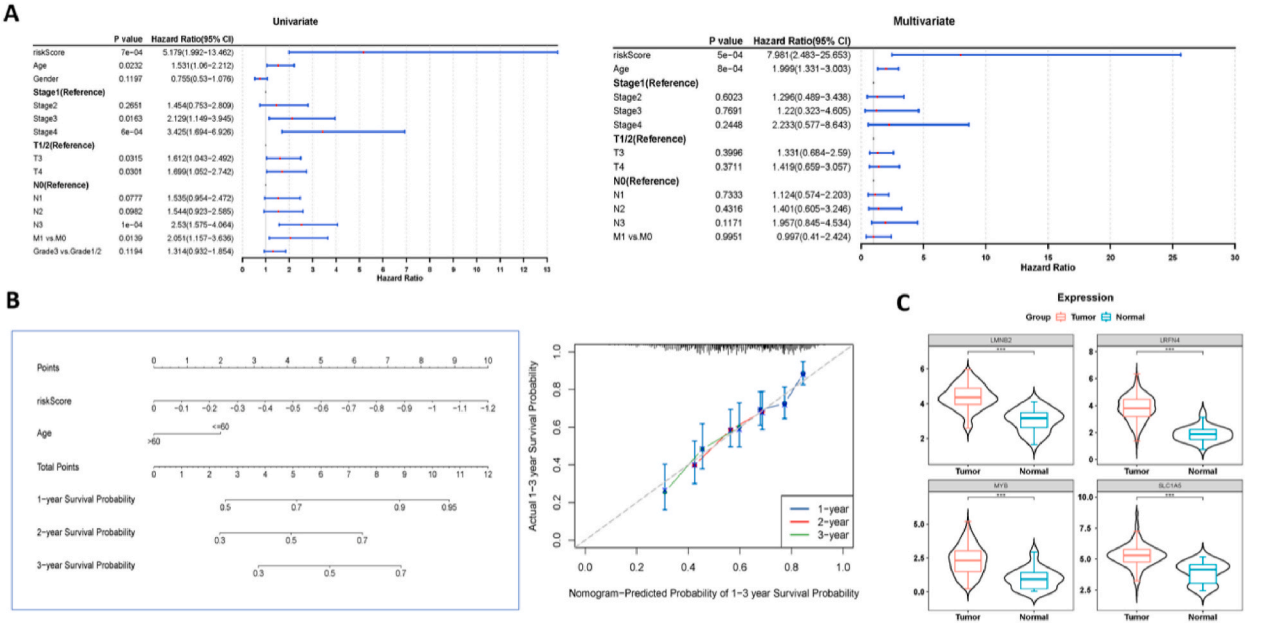

Fig. 8. Nomogram model construction and evaluation. (A) Forest plots for hazard ratios (HRs) of the risk score, together with age, gender, stages and TNM staging system in GC in the TCGA-STAD dataset. The left panel shows the results from the univariate Cox regression analysis, while the right panel shows the multivariate Cox regression analysis. (B) The 1-/2-/3-year survival prognostic nomogram includes the risk score and age (Left panel). The calibration curves of nomogram prediction possibility vs. the actual possibility of survivals. The grey line represents a perfect prediction of the nomogram. (C) Expression analysis of risk model genes, where red indicates tumor, sky blue indicates normal "***", $P < 0.001$. (For interpretation of the references to color in this figure legend, the reader is referred to the Web version of this article.)

types, and is over-expressed in various cancer tissues and is associated with poor prognosis [28]. The CD36-BATF2/MYB axis demonstrates a substantial predictive efficacy for the response to anti-PD-1 drugs during the treatment of GC [29]. *LRFN4* (leucine rich repeat and fibronectin type III domain containing 4) gene encodes a member of the LRFN family protein, which is a membrane molecule with tyrosine kinase activity and rich in leucine and participates in the formation of extracellular matrix and cell migration [30]. Upregulation of LRFN4 leads to decreased adhesion of tumor cells, thereby promoting tumor invasion and metastasis [31]. The expression of LRFN4 is up-regulated in tumor tissues and correlates with the high TNM stages, lymph node metastasis, and poor prognosis in colon cancer [32]. However, one study has found that the up-regulated expression of LRFN4 is not related with the poor prognosis of GC [33], thus the specific mechanism of *LRFN4* needs further exploration. *LMNB2* gene encodes a B type nuclear lamin (Lamin B2), which belongs to the nuclear lamin family that is critical in keeping the integrity of nuclear envelope and nucleolus and is involved in cell proliferation and aging, DNA damage repair and gene expression [34]. LMNB2 is pivotal in tumorigenesis and progress, and its abnormal expression is associated with colorectal cancer, HCC, lung cancer, bladder cancer and breast cancer. The specific mechanisms accounting for the function of LMNB2 include DNA methylation, chromosomal instability, abnormal cell cycle, epithelial-mesenchymal transition (EMT) and changes in DNA replication activity [35]. The present study may have for the first time provided a clue that LMNB2 may affect the progression of GC. *SLC1A5* (Solute carrier family 1 member 5) gene encodes a protein also called ASCT2 (Alanine, Serine, Cysteine transporter 2), which is a membrane-localized glutamine transporter that promotes cancer growth by activating glutamine metabolism in tumor cells [36]. SLC1A5 is overexpressed in various cancers including GC, and knockdown of *SLC1A5* can inhibit glutamine uptake and the growth of GC cells [37].

In the present study, we have applied GO and KEGG enrichment analyses using R package GSVA, dividing the disease samples into high- and low-risk groups based on the risk scores. The high-risk group genes were mainly related to the calcium signaling pathway, extracellular matrix (ECM) receptor interaction and other functional pathways. The remodeling of ECM, i.e. the synthesis, distribution and degradation of ECM, greatly contributes to cancer metastasis [38]. For instance, the progression of colon cancer is regulated by the ECM molecule EMILIN-2, which affects macrophage polarization through the TLR-4/MyD88 pathway [39]. ECM components are also involved in the tumorigenesis, progression and poor survival of GC [40]. The Ca^{2+} signal transduction pathway takes a critical role in metastasis of GC cells, and the expression level of calcium release-activated calcium regulator 2 (ORAI2) was increased in metastatic GC and enhanced the tumorigenicity of GC by activating SOC activity through PI3K/Akt signaling pathway [40]. ORAI2 was found to be able to reinforce the ability to metastasize and invade of GC cells by inducing FAK-mediated MAPK/ERK activation [41].

On the other hand, the low-risk patent genes were primarily enriched in the positive modulation of chromosome segregation, DNA replication in mitosis and nucleotide excision repair. Chromosome segregation is a critical process in cell division, and errors in chromosome segregation during cell division can lead to the expansion of cancer [42]. DNA replication failure is one of the major causes of genome instability, which can lead to aneuploidy, chromosome breakage, and chromosomal rearrangements [43]. The deficiency of nucleotide excision repair can increase the instability and integrity of the genome, and its polymorphism may alter the

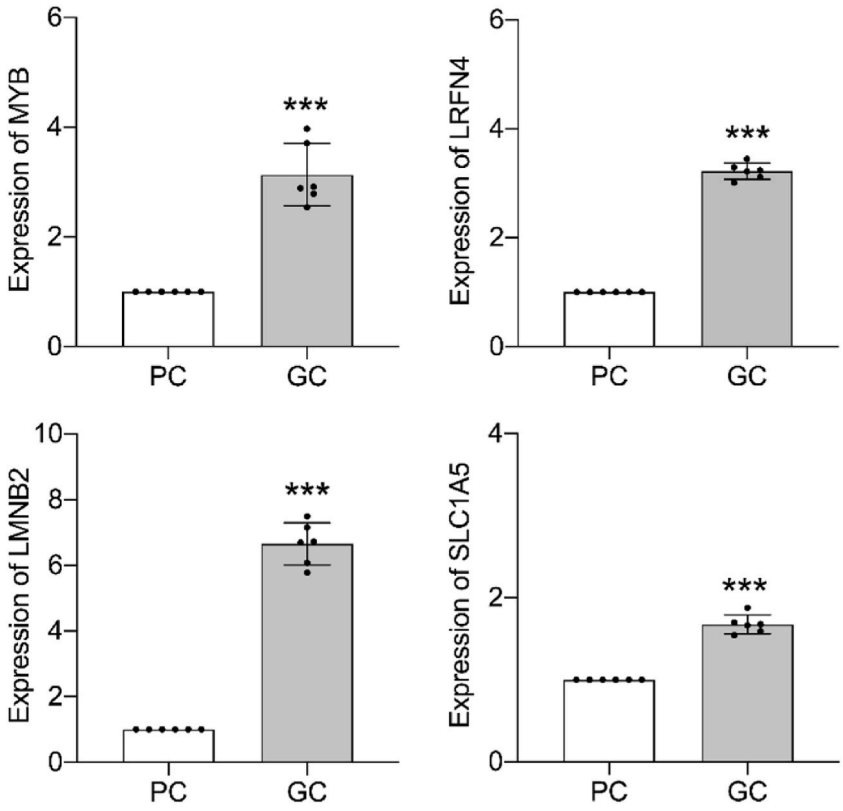

Fig. 9. Four risk model genes (MYB, LRFN4, LMNB2, and SLC1A5) were detected in gastric cancer (GC) and para-carcinoma tissue (PC) by qRT-PCR analysis(***, $p < 0.05$).

ability of NER by affecting the expression and function of key proteins, thereby changing an individual's susceptibility to GC and triggering tumorigenesis [44].

Immunotherapy is one of the most promising cancer treatments, as it turns the power of the immune system against cancer cells. Herin, we have analyzed the correlation of the novel risk model with tumor immune microenvironments of GC, and found that the proportions of immune cells, like activated $CD4^+$ T cells, and immune checkpoints, such as *C10orf54*, significantly differed between the high- and low-risk groups. It is well acknowledged that $CD4^+$ T cells can assist in immune responses. It has been reported that glutamine metabolism controls the transformation of $CD4^+$ T cells into inflammatory subtypes and immune cells activation, thus altering cancer immune microenvironments in GC [45]. There was a significant positive correlation between *C10orf54* (encoding VISTA [V-domain Ig suppressor of T cell activation] protein) and genes responsible for immune escape and immunosuppression in colorectal cancer [46]. CD200 is a member of the immunoglobulin superfamily that interacts with its receptor CD200R1 to regulate tumor immune microenvironments. The immunosuppressive mechanism driven via the CD200R/CD200 interaction involves suppressing macrophages, inducing regulatory T cells, shifting cytokines profile from Th1 to Th2, inhibiting tumor-specific T cell immunity, and activating myeloid cells [47]. *LRFN4* is involved in the migration of macrophages into inflammatory areas and the polarization of M2 macrophages, which are associated with a poor prognosis in lung adenocarcinoma [48]. Overexpression of *SLC1A5* can enhance the metabolic capacity and effector function of CAR-NK/T cells in tumor immunotherapy [49], while its down-regulation curtails tumor-associated macrophage infiltration and M2 polarization in glioma [50].

It is crucial to use an effective risk evaluation system for successful screening the GC high-risk people so that certain diagnostic methods can be applied precisely on this population, and early diagnosis and treatment could become possible. At present, the comprehensive evaluation system includes clinical variables, serum markers, and risk prediction system based on gene expression and polymorphism [51]. The glutamine metabolism risk module generated in this study, along with "age", was validated as the independent prognostic factor for GC through Cox multivariate and univariate analyses. The nomogram showed both factors had a strong predictive ability for the survival of GC patients. In support, "age" has already been regarded as a useful predictive indicator for GC. The incidence and mortality of GC increase among individuals aged over 40 years, peaking at 65 years globally; patients under 40 years old had more stable diseases, higher chances of receiving systemic treatments, and longer survival time than those over 65 years old [52].

In conclusion, this study has identified a novel risk model consisting of four GMRGs (*MYB*, *LRFN4*, *LMNB2*, and *SLC1A5*) in GC using multiple and comprehensive analyses. These genes were involved in functional pathways and were over-expressed in tumor tissues. The risk model was shown to be strongly correlated with oncogenic pathways, particularly with metabolism-related pathways.

Most importantly, this risk model was related to factors composing tumor immune microenvironments, such as immune effector cells, response gene sets and checkpoints, and correlated with immune checkpoint blockade therapy. Finally, this risk model, along with "age", was validated as an independent prognostic factor for GC. Unfortunately, the present study has several limitations that need to be addressed in the future. One limitation is the relatively small sample size due to the availability of public databases. In addition, the results have not been verified in cell and animal experiments or in clinical studies. In the future, we will focus on expanding the geographical and demographic diversity of our sample population by integrating multicenter clinical trials and leveraging extensive public database resources to ensure the generalizability of our research findings. Additionally, we will incorporate cell-based assays and animal models to verify the expression patterns of glutamine metabolism-related genes observed clinically and their correlation with prognosis. This approach will provide experimental evidence for a deeper exploration of the potential mechanisms and the identification of potential therapeutic targets. Ultimately, this study aims to integrate multi-omics assay, including transcriptomics, genomics, metabolomics, and proteomics to further elucidate the role of glutamine metabolism in gastric cancer. By uncovering the complex molecular mechanisms underlying tumorigenesis, progression, and treatment response, this research will provide a robust scientific foundation for the molecular pathology of gastric cancer and lay the groundwork for developing new therapeutic strategies. Therefore, the discovery of this novel risk model and its component genes based on glutamine metabolism warrants further investigation, since it is likely to promote the current systems for predicting the prognosis and monitoring the response to immune checkpoint blockade treatments, and may also serve as a potential linkage to therapeutic options for combating GC.

Ethics approval and consent to participate

The study was conducted in strict accordance with the principles outlined in the World Medical Association Declaration of Helsinki. This study was reviewed and approved by [Ethics Committee of Zhongshan City People's Hospital] with the approval number: [2023-070], dated [2023-11-01], and informed consent was secured from all participating patients.

Funding sources

This work was supported by the Guangdong High-level Hospital Construction Fund at Zhongshan City People's Hospital (SG2002005) and Guangdong Medical Science and Technology Research Foundation (No. B2020085).

Data availability statement

The data analyzed in this study were obtained from public databases. In the TCGA database (https://cancergenome.nih.gov/abouttcga/overview), GEO database (https://www.ncbi.nlm.nih.gov/gds), MSigDB (https://www.gsea-msigdb.org/gsea/msigdb/index.jsp) and GeneCard database (href="https://genecards.weizmann.ac.il/v3/"title = "https://genecards.weizmann.ac.il/v3/ ">https://genecards.weizmann.ac.il/v3/).

CRediT authorship contribution statement

Weidong Li: Writing – original draft, Funding acquisition. **Qixing Zhong:** Software, Data curation. **Naisheng Deng:** Software, Data curation. **Haitao Wang:** Methodology, Formal analysis. **Jun Ouyang:** Software, Methodology, Formal analysis. **Zhifen Guan:** Software, Methodology, Formal analysis. **Xinhao Zhou:** Methodology, Formal analysis. Li K performed the experiments of qRT-PCR. **Xueying Sun:** Writing – review & editing, Conceptualization. **Yao Wang:** Writing – review & editing, Supervision, Conceptualization.

Declaration of competing interest

The authors declare that they have no known competing financial interests or personal relationships that could have appeared to influence the work reported in this paper.

Acknowledgment

None.

Appendix A. Supplementary data

Supplementary data to this article can be found online at https://doi.org/10.1016/j.heliyon.2024.e37985.

References

[1] R.L. Siegel, K.D. Miller, H.E. Fuchs, A. Jemal, Cancer statistics, CA Cancer J Clin 71 (1) (2021) 7–33, https://doi.org/10.3322/caac.21654.

[2] H. Sung, J. Ferlay, R.L. Siegel, M. Laversanne, I. Soerjomataram, A. Jemal, et al., Global cancer statistics 2020: GLOBOCAN Estimates of incidence and mortality worldwide for 36 cancers in 185 countries, CA Cancer J Clin 71 (3) (2021) 209–249, https://doi.org/10.3322/caac.21660.

[3] E.C. Smyth, M. Nilsson, H.I. Grabsch, N.C. van Grieken, F. Lordick, Gastric cancer, Lancet. 396 (10251) (2020) 635–648, https://doi.org/10.1016/s0140-6736(20)31288-5.

[4] W.L. Guan, Y. He, R.H. Xu, Gastric cancer treatment: recent progress and future perspectives, J. Hematol. Oncol. 16 (1) (2023) 57, https://doi.org/10.1186/s13045-023-01451-3.

[5] L. Vettore, R.L. Westbrook, D.A. Tennant, New aspects of amino acid metabolism in cancer, Br. J. Cancer 122 (2) (2020) 150–156, https://doi.org/10.1038/s41416-019-0620-5.

[6] H. Tapiero, G. Mathé, P. Couvreur, K.D. Tew, II. Glutamine and glutamate, Biomed. Pharmacother. 56 (9) (2002) 446–457, https://doi.org/10.1016/s0753-3322(02)00285-8.

[7] T. Li, C. Copeland, A. Le, Glutamine metabolism in cancer, Adv. Exp. Med. Biol. 1311 (2021) 17–38, https://doi.org/10.1007/978-3-030-65768-0_2.

[8] A.R. Mullen, W.W. Wheaton, E.S. Jin, P.H. Chen, L.B. Sullivan, T. Cheng, et al., Reductive carboxylation supports growth in tumour cells with defective mitochondria, Nature 481 (7381) (2011) 385–388, https://doi.org/10.1038/nature10642.

[9] R.D. Leone, L. Zhao, J.M. Englert, I.M. Sun, M.H. Oh, I.H. Sun, et al., Glutamine blockade induces divergent metabolic programs to overcome tumor immune evasion, Science 366 (6468) (2019) 1013–1021, https://doi.org/10.1126/science.aav2588.

[10] B.J. Altman, Z.E. Stine, C.V. Dang, From Krebs to clinic: glutamine metabolism to cancer therapy, Nat. Rev. Cancer 16 (10) (2016) 619–634, https://doi.org/10.1038/nrc.2016.71.

[11] W.H. Yang, Y. Qiu, O. Stamatatos, T. Janowitz, M.J. Lukey, Enhancing the efficacy of glutamine metabolism inhibitors in cancer therapy, Trends Cancer 7 (8) (2021) 790–804, https://doi.org/10.1016/j.trecan.2021.04.003.

[12] S. Huang, Y. Guo, Z. Li, Y. Zhang, T. Zhou, W. You, et al., A systematic review of metabolomic profiling of gastric cancer and esophageal cancer, Cancer Biol Med 17 (1) (2020) 181–198, https://doi.org/10.20892/j.issn.2095-3941.2019.0348.

[13] A. Hirayama, K. Kami, M. Sugimoto, M. Sugawara, N. Toki, H. Onozuka, et al., Quantitative metabolome profiling of colon and stomach cancer microenvironment by capillary electrophoresis time-of-flight mass spectrometry, Cancer Res. 69 (11) (2009) 4918–4925, https://doi.org/10.1158/0008-5472.Can-08-4806.

[14] H. Ma, J. Wu, M. Zhou, J. Wu, Z. Wu, L. Lin, et al., Inhibition of glutamine uptake improves the efficacy of Cetuximab on gastric cancer, Integr. Cancer Ther. 20 (2021) 15347354211045349, https://doi.org/10.1177/15347354211045349.

[15] S.S. Joshi, B.D. Badgwell, Current treatment and recent progress in gastric cancer, CA Cancer J Clin 71 (3) (2021) 264–279, https://doi.org/10.3322/caac.21657.

[16] K.C. Kao, S. Vilbois, C.H. Tsai, P.C. Ho, Metabolic communication in the tumour-immune microenvironment, Nat. Cell Biol. 24 (11) (2022) 1574–1583, https://doi.org/10.1038/s41556-022-01002-x.

[17] S. He, S. Zhang, Y. Yao, B. Xu, Z. Niu, F. Liao, et al., Turbulence of glutamine metabolism in pan-cancer prognosis and immune microenvironment, Front. Oncol. 12 (2022) 1064127, https://doi.org/10.3389/fonc.2022.1064127.

[18] S. Liu, Z. Wang, R. Zhu, F. Wang, Y. Cheng, Y. Liu, Three differential expression analysis methods for RNA sequencing: limma, EdgeR, DESeq2, J. Vis. Exp. 175 (2021), https://doi.org/10.3791/62528.

[19] G. Yu, L.G. Wang, Y. Han, Q.Y. He, clusterProfiler: an R package for comparing biological themes among gene clusters, OMICS 16 (5) (2012) 284–287, https://doi.org/10.1089/omi.2011.0118.

[20] Q. Xu, S. Chen, Y. Hu, W. Huang, Landscape of immune microenvironment under immune cell infiltration pattern in breast cancer, Front. Immunol. 12 (2021) 711433, https://doi.org/10.3389/fimmu.2021.711433.

[21] R. Su, C. Jin, H. Bu, J. Xiang, L. Zhou, C. Jin, Development and validation of an immune-related prognostic signature in cervical cancer, Front. Oncol. 12 (2022) 861392, https://doi.org/10.3389/fonc.2022.861392.

[22] T. Mosmann, Rapid colorimetric assay for cellular growth and survival: application to proliferation and cytotoxicity assays, J. Immunol. Methods 65 (1–2) (1983) 55–63, https://doi.org/10.1016/0022-1759(83)90303-4.

[23] S. Ning, W. Wei, J. Li, B. Hou, J. Zhong, Y. Xie, et al., Clinical significance and diagnostic capacity of serum TK1, CEA, CA 19-9 and CA 72-4 levels in gastric and colorectal cancer patients, J. Cancer 9 (3) (2018) 494–501, https://doi.org/10.7150/jca.21562.

[24] M. Suzuki, H. Toki, A. Furuya, H. Ando, Establishment of monoclonal antibodies against cell surface domains of ASCT2/SLC1A5 and their inhibition of glutamine-dependent tumor cell growth, Biochem. Biophys. Res. Commun. 482 (4) (2017) 651–657, https://doi.org/10.1016/j.bbrc.2016.11.089.

[25] J. Liao, P.P. Liu, G. Hou, J. Shao, J. Yang, K. Liu, et al., Regulation of stem-like cancer cells by glutamine through β-catenin pathway mediated by redox signaling, Mol. Cancer 16 (1) (2017) 51, https://doi.org/10.1186/s12943-017-0623-x.

[26] J. Ye, Q. Huang, J. Xu, J. Huang, J. Wang, W. Zhong, et al., Targeting of glutamine transporter ASCT2 and glutamine synthetase suppresses gastric cancer cell growth, J. Cancer Res. Clin. Oncol. 144 (5) (2018) 821–833, https://doi.org/10.1007/s00432-018-2605-9.

[27] S. Battista, M.R. Ambrosio, F. Limarzi, G. Gallo, L. Saragoni, Molecular alterations in gastric Preneoplastic lesions and early gastric cancer, Int. J. Mol. Sci. 22 (13) (2021), https://doi.org/10.3390/ijms22136652.

[28] Y. Cicirò, A. Sala, MYB oncoproteins: emerging players and potential therapeutic targets in human cancer, Oncogenesis 10 (2) (2021) 19, https://doi.org/10.1038/s41389-021-00309-y.

[29] Q. Jiang, Z. Chen, F. Meng, H. Zhang, H. Chen, J. Xue, et al., CD36-BATF2\MYB Axis predicts anti-PD-1 immunotherapy response in gastric cancer, Int. J. Biol. Sci. 19 (14) (2023) 4476–4492, https://doi.org/10.7150/ijbs.87635.

[30] J. Nam, W. Mah, E. Kim, The SALM/Lrfn family of leucine-rich repeat-containing cell adhesion molecules, Semin. Cell Dev. Biol. 22 (5) (2011) 492–498, https://doi.org/10.1016/j.semcdb.2011.06.005.

[31] Y. Liu, X. Chen, X. Chen, X. Yang, Q. Song, H. Wu, High SALM3 expression in tumor cells and fibroblasts is correlated with poor prognosis in gastric cancer patients, Dis. Markers 2019 (2019) 8282414, https://doi.org/10.1155/2019/8282414.

[32] F. Zheng, X.L. Zhai, W.J. Wang, K.P. Guo, C.C. Xiao, Q.C. Ni, [Expression and clinical significance of LRFN4 in colorectal cancer tissue], Zhonghua Yixue Zazhi 100 (22) (2020) 1745–1749, https://doi.org/10.3760/cma.j.cn112137-20190905-01975.

[33] S. Han, W. Zhu, W. Yang, Q. Guan, C. Chen, Q. He, et al., A prognostic signature constructed by CTHRC1 and LRFN4 in stomach adenocarcinoma, Front. Genet. 12 (2021) 646818, https://doi.org/10.3389/fgene.2021.646818.

[34] A. Sen Gupta, K. Sengupta, Lamin B2 modulates nucleolar morphology, dynamics, and function, Mol. Cell Biol. 37 (24) (2017), https://doi.org/10.1128/mcb.00274-17.

[35] C. Evangelisti, I. Rusciano, S. Mongiorgi, G. Ramazzotti, G. Lattanzi, L. Manzoli, et al., The wide and growing range of lamin B-related diseases: from laminopathies to cancer, Cell. Mol. Life Sci. 79 (2) (2022) 126, https://doi.org/10.1007/s00018-021-04084-2.

[36] J. Lin, T. Yang, Z. Peng, H. Xiao, N. Jiang, L. Zhang, et al., SLC1A5 silencing inhibits esophageal cancer growth via cell cycle arrest and apoptosis, Cell. Physiol. Biochem. 48 (1) (2018) 397, https://doi.org/10.1159/000491769.

[37] L. Wang, Y. Liu, T.L. Zhao, Z.Z. Li, J.Y. He, B.J. Zhang, et al., Topotecan induces apoptosis via ASCT2 mediated oxidative stress in gastric cancer, Phytomedicine 57 (2019) 117–128, https://doi.org/10.1016/j.phymed.2018.12.011.

[38] C. Bonnans, J. Chou, Z. Werb, Remodelling the extracellular matrix in development and disease, Nat. Rev. Mol. Cell Biol. 15 (12) (2014) 786–801, https://doi.org/10.1038/nrm3904.

[39] E. Andreuzzi, A. Fejza, M. Polano, E. Poletto, L. Camicia, G. Carobolante, et al., Colorectal cancer development is affected by the ECM molecule EMILIN-2 hinging on macrophage polarization via the TLR-4/MyD88 pathway, J. Exp. Clin. Cancer Res. 41 (1) (2022) 60, https://doi.org/10.1186/s13046-022-02271-y.

[40] J. Zhu, C. Luo, J. Zhao, X. Zhu, K. Lin, F. Bu, et al., Expression of LOX suggests poor prognosis in gastric cancer, Front. Med. 8 (2021) 718986, https://doi.org/10.3389/fmed.2021.718986.

[41] Y. Ye, X. Li, Z. Wang, F. Ye, W. Xu, R. Lu, et al., 3,3'-Diindolylmethane induces gastric cancer cells death via STIM1 mediated store-operated calcium entry, Int. J. Biol. Sci. 17 (5) (2021) 1217–1233, https://doi.org/10.7150/ijbs.56833.
[42] S.J. Klaasen, M.A. Truong, R.H. van Jaarsveld, I. Koprivec, V. Štimac, S.G. de Vries, et al., Nuclear chromosome locations dictate segregation error frequencies, Nature 607 (7919) (2022) 604–609, https://doi.org/10.1038/s41586-022-04938-0.
[43] E.A. Epum, J.E. Haber, DNA replication: the recombination connection, Trends Cell Biol. 32 (1) (2022) 45–57, https://doi.org/10.1016/j.tcb.2021.07.005.
[44] J. He, Z.J. Zhuo, A. Zhang, J. Zhu, R.X. Hua, W.Q. Xue, et al., Genetic variants in the nucleotide excision repair pathway genes and gastric cancer susceptibility in a southern Chinese population, Cancer Manag. Res. 10 (2018) 765–774, https://doi.org/10.2147/cmar.S160080.
[45] L. Zhao, Y. Liu, S. Zhang, L. Wei, H. Cheng, J. Wang, et al., Impacts and mechanisms of metabolic reprogramming of tumor microenvironment for immunotherapy in gastric cancer, Cell Death Dis. 13 (4) (2022) 378, https://doi.org/10.1038/s41419-022-04821-w.
[46] S. Xie, J. Huang, Q. Qiao, W. Zang, S. Hong, H. Tan, et al., Expression of the inhibitory B7 family molecule VISTA in human colorectal carcinoma tumors, Cancer Immunol. Immunother. 67 (11) (2018) 1685–1694, https://doi.org/10.1007/s00262-018-2227-8.
[47] K. Kotwica-Mojzych, B. Jodłowska-Jędrych, M. Mojzych, CD200:CD200R interactions and their importance in immunoregulation, Int. J. Mol. Sci. 22 (4) (2021), https://doi.org/10.3390/ijms22041602.
[48] G.C. Wang, M. Zhou, Y. Zhang, H.M. Cai, S.T. Chiang, Q. Chen, et al., Screening and identifying a novel M-MDSCs-related gene signature for predicting prognostic risk and immunotherapeutic responses in patients with lung adenocarcinoma, Front. Genet. 13 (2022) 989141, https://doi.org/10.3389/fgene.2022.989141.
[49] M. Nachef, A.K. Ali, S.M. Almutairi, S.H. Lee, Targeting SLC1A5 and SLC3A2/SLC7A5 as a potential strategy to strengthen anti-tumor immunity in the tumor microenvironment, Front. Immunol. 12 (2021) 624324, https://doi.org/10.3389/fimmu.2021.624324.
[50] L. Han, J. Zhou, L. Li, X. Wu, Y. Shi, W. Cui, et al., SLC1A5 enhances malignant phenotypes through modulating ferroptosis status and immune microenvironment in glioma, Cell Death Dis. 13 (12) (2022) 1071, https://doi.org/10.1038/s41419-022-05526-w.
[51] X.Y. Wang, L.L. Wang, L. Xu, S.Z. Liang, M.C. Yu, Q.Y. Zhang, et al., Evaluation of polygenic risk score for risk prediction of gastric cancer, World J. Gastrointest. Oncol. 15 (2) (2023) 276–285, https://doi.org/10.4251/wjgo.v15.i2.276.
[52] W. Cao, H.D. Chen, Y.W. Yu, N. Li, W.Q. Chen, Changing profiles of cancer burden worldwide and in China: a secondary analysis of the global cancer statistics 2020, Chin Med J (Engl). 134 (7) (2021) 783–791, https://doi.org/10.1097/cm9.0000000000001474.